nature structural & molecular biology

Conformational dynamics of single pre-mRNA molecules during *in vitro* splicing

John Abelson[1,6], Mario Blanco[2,6], Mark A Ditzler[3–5], Franklin Fuller[3,4], Pavithra Aravamudhan[3,4], Mona Wood[3], Tommaso Villa[1,5], Daniel E Ryan[1,5], Jeffrey A Pleiss[1,5], Corina Maeder[1], Christine Guthrie[1] & Nils G Walter[3]

The spliceosome is a complex small nuclear RNA (snRNA)-protein machine that removes introns from pre-mRNAs via two successive phosphoryl transfer reactions. The chemical steps are isoenergetic, yet splicing requires at least eight RNA-dependent ATPases responsible for substantial conformational rearrangements. To comprehensively monitor pre-mRNA conformational dynamics, we developed a strategy for single-molecule FRET (smFRET) that uses a small, efficiently spliced yeast pre-mRNA, Ubc4, in which donor and acceptor fluorophores are placed in the exons adjacent to the 5′ and 3′ splice sites. During splicing *in vitro*, we observed a multitude of generally reversible time- and ATP-dependent conformational transitions of individual pre-mRNAs. The conformational dynamics of branchpoint and 3′–splice site mutants differ from one another and from wild type. Because all transitions are reversible, spliceosome assembly appears to be occurring close to thermal equilibrium.

Introns in eukaryotic pre-mRNAs are removed by RNA splicing. This process is carried out by the spliceosome, a large supramolecular assembly consisting of five small nuclear RNAs and more than 100 proteins[1,2]. The spliceosome lacks a preformed catalytic core; rather, spliceosomes are assembled on intron-containing substrates in a stepwise manner that requires both binding and release of small nuclear ribonucleoproteins (snRNPs; reviewed in ref. 2). Notably, splicing entails two successive phosphoryl transfer reactions that are isoenergetic. Nonetheless, spliceosome assembly requires at least eight RNA-dependent ATPases of the so-called 'DEAD-box' (DExD/H) family[3]. These enzymes, which catalyze successive rearrangements of RNA and protein pairing partners, are believed to enhance the fidelity of splicing by acting as proofreading clocks to allow the discarding of mutant substrates at multiple steps in the assembly and catalytic pathway[4–7].

In the budding yeast *Saccharomyces cerevisiae*, assembly (reviewed in ref. 2) is initiated by the ATP-independent formation of a commitment complex, in which the U1 snRNP interacts with the 5′ splice site while branchpoint binding protein and the splicing factor Mud2 interact with the branchpoint sequence (**Fig. 1**). If the branchpoint is mutated, this complex cannot form and spliceosome assembly is blocked. With a wild-type (WT) precursor, the commitment complex is converted to the pre-spliceosome by the ATP-dependent binding of U2 to the branchpoint, followed by association of the U4/U6.U5 triple snRNP. Before the first transesterification can occur, U1 and U4 snRNPs must be released from the assembled spliceosome, again in ATP-dependent reactions. Importantly, the first chemical step, which results in formation of the lariat intermediate and free 5′ exon, can occur even in the presence of a mutation at the 3′ splice site. This mutation specifically blocks the second transesterification. Finally, the spliceosome undergoes ATP-dependent disassembly from the lariat intron and mature mRNA (**Fig. 1**).

Despite this level of understanding of the pathway, major questions about the specific conformational rearrangements, and particularly their kinetics (and splicing-signal dependence), remain unanswered. This gap in our knowledge is in large part due to the fact that, to date, splicing must be studied in a crude extract *in vitro*, where multistep reversible processes are obscured by asynchronous progression along the pathway[8]. In addition, splicing in a yeast extract is generally inefficient, leading only a fraction of molecules to undergo one or both steps of splicing. To overcome these severe limitations and monitor in real time the conformational states of the pre-mRNA in spliceosome assembly, we have developed an *in vitro* assay based on single-molecule fluorescence resonance energy transfer (smFRET) that obviates the need to isolate or synchronize reaction intermediates.

We first identified a natural yeast pre-mRNA, Ubc4, with a small intron that is efficiently spliced *in vitro*. This made possible the chemical synthesis of the pre-mRNA with donor (Cy3) and acceptor (Cy5) fluorophores in the exons adjacent to the 5′ and 3′ splice sites, respectively. The Förster radius of the Cy3-Cy5 fluorophore pair is ~54 Å, so that smFRET can effectively monitor changes in inter-fluorophore distance between ~20–100 Å. Electron cryomicroscopy

[1]Department of Biochemistry and Biophysics, University of California, San Francisco, San Francisco, California, USA. [2]Department of Cellular and Molecular Biology, [3]Department of Chemistry and [4]Department of Biophysics, Single Molecule Analysis Group, University of Michigan, Ann Arbor, Michigan, USA. [5]Present addresses: Department of Microbiology and Immunology, University of Missouri Medical School, Columbia, Missouri, USA (M.A.D.); Centre de Génétique Moléculaire, Centre National de la Recherche Scientifique, Gif sur Yvette, France (T.V.); Agilent Technologies, Santa Clara, California, USA (D.E.R.); Department of Molecular Biology and Genetics, Cornell University, Ithaca, New York, USA (J.A.P.). [6]These authors contributed equally to this work. Correspondence should be addressed to J.A. (johnabelson@gmail.com) or N.G.W. (nwalter@umich.edu).

Received 22 March 2009; accepted 16 December 2009; published online 21 March 2010; doi:10.1038/nsmb.1767

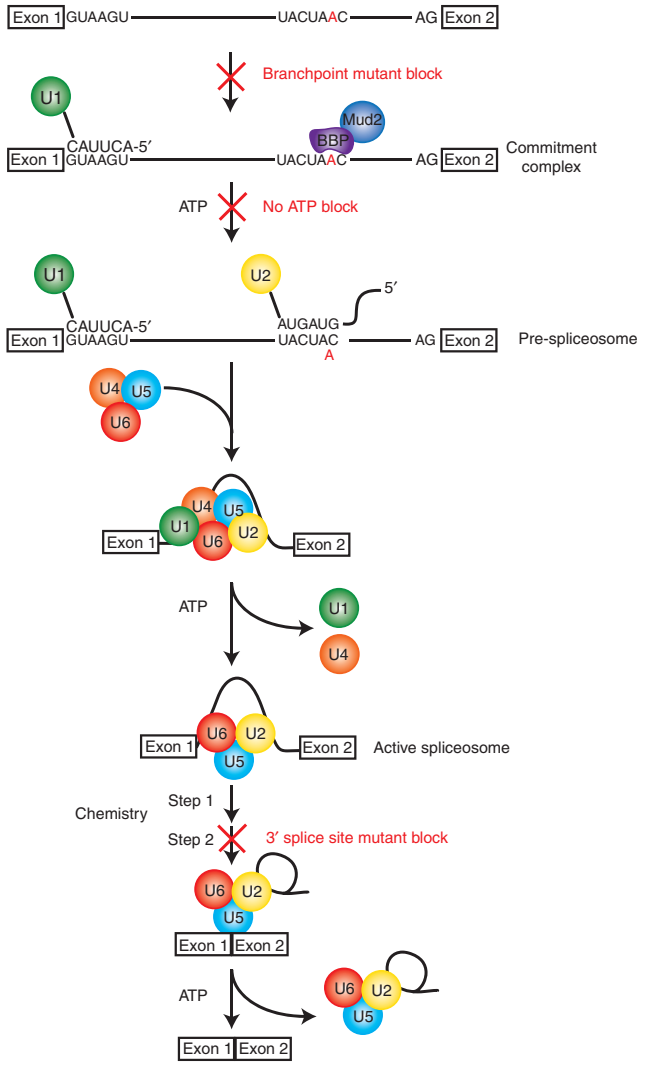

Figure 1 Canonical spliceosome assembly pathway.

micrographs of snRNPs and spliceosomal complexes range in size from 200–300 Å (refs. 9,10), yet cross-linking and footprinting indicate proximity of the two exons throughout splicing[11,12]. Using total internal reflection fluorescence microscopy (TIRFM) of immobilized Ubc4, we show here that the pre-mRNA reversibly folds into conformations with proximal exons, even in the absence of splicing extract. Spliceosome assembly further accelerates and diversifies these conformational dynamics. We establish four criteria that suggest that we are indeed monitoring spliceosome assembly at the level of single molecules: the surface-immobilized pre-mRNA is efficiently spliced, as verified by an *in situ* assay; the observed complex smFRET transitions are time- and ATP-dependent; and those transitions are dependent on appropriate intron signals. Our results suggest that the spliceosome is a cellular machine that operates close to equilibrium, like the ribosome.

RESULTS

Identification and characterization of a suitable pre-mRNA

In *Saccharomyces cerevisiae*, most *in vitro* splicing assays have used the ~1,400-nucleotide (nt) actin pre-mRNA (with an intron of 308 nt)[13]. To develop our smFRET approach, however, we sought to identify a smaller pre-mRNA, efficiently spliced *in vitro*, that would be amenable to chemical synthesis. To this end, we analyzed pre-mRNAs from the temperature-sensitive yeast mutant *prp2-1* (ref. 14).

In this mutant, splicing is blocked before the first catalytic step when cells are shifted to the nonpermissive temperature, resulting in the efficient accumulation of most yeast pre-mRNAs[15,16]. We extracted total RNA from *prp2-1* cells grown first at permissive temperature (30 °C) and then shifted for 30 min to the nonpermissive temperature (37 °C). Previous experiments had shown that this RNA preparation contains pre-mRNAs from most genes containing introns and a small background of mature mRNAs spliced during the permissive growth period[16]. We subjected this RNA mixture to *in vitro* splicing conditions in yeast cell extract, isolated it and analyzed it using a splicing microarray that could detect mature, spliced mRNAs[16]. Several efficiently spliced candidates with small introns were identified (**Supplementary Table 1**). We ultimately chose the pre-mRNA for *UBC4* as the most suitable substrate for our smFRET analysis.

The entire *UBC4* gene is 542 nt long, with a short intron of 95 nt. We synthesized a number of Ubc4 pre-mRNAs with different exon lengths and assayed their splicing activity (**Fig. 2**). In a trade-off between ease of synthesis and splicing activity of the substrate, we chose to develop a variant of the Ubc4 pre–mRNA for smFRET consisting of 20-nt exons and the 95-nt intron for a total size of 135 nt. We prepared this truncated Ubc4 pre-mRNA through a two-piece ligation of synthesized RNAs (see Online Methods). We postsynthetically coupled the donor fluorophore Cy3 to the 5′ exon and the acceptor Cy5 to the 3′ exon, seeking to place the fluorophores as close as possible to the 5′ and 3′ splice sites, respectively, for maximum distance sensitivity without interfering with splicing activity. We prepared pre-mRNAs with dyes located at uridines in multiple positions, all of which are spliced with a similar efficiency of ~30–40% (**Fig. 2a**). The substrate used in this work carries Cy3 in exon 1, 7 nt from the 5′ splice site, and Cy5 in exon 2, 4 nt from the 3′ splice site (**Fig. 2a**). Introduction of the 3′–splice site mutation (3′SS) or the branchpoint mutation (BP) into this smFRET substrate was found to have the expected effects[17] of blocking splicing before the second and first steps of splicing, respectively (**Fig. 2b**).

In our smFRET assays, we immobilized the 3′ end of the labeled pre-mRNA through hybridization to a short 2′-*O*-methyl capture RNA with a 5′ biotin, which was bound to a streptavidin-coated and PEG-passivated quartz slide (**Fig. 3a**). Hybridization of the capture RNA to Ubc4 pre-mRNA did not affect the efficiency of splicing in ensemble assays (data not shown). We detected the Cy3 and Cy5 fluorophores by TIRFM in real time to determine the smFRET efficiency, as described previously[8,18–21]. By using TIRFM, we minimized the background fluorescence of the splicing extract but still captured all sufficiently long-lived conformational states of the pre-mRNA (even in a fully extended pre-mRNA of ~50 nm, the distal Cy3 dye is still well within the ~100-nm-deep evanescent light field of TIRFM[8]). We used an enzymatic oxygen scavenger system to limit photobleaching and added Trolox to suppress fluorophore blinking (see Online Methods). Ensemble splicing assays showed that the presence of the oxygen scavenger system and Trolox in the reaction mix did not inhibit splicing (data not shown). Under these conditions, we observed limited quenching, blinking and photobleaching, with rate constants of ~0.01 s^{-1}. These effects were the same for each of the three pre-mRNAs, and we found no appreciable change in the quenching/blinking and photobleaching upon addition of ATP.

To verify that the spliceosome assembles on the immobilized pre-mRNA to remove its intron, we performed an *in situ* RNase H sensitivity assay under our TIRFM conditions (**Supplementary Fig. 1**). Briefly, we added a DNA oligonucleotide complementary to the intron, together with RNase H, to slides on which WT pre-mRNA had been

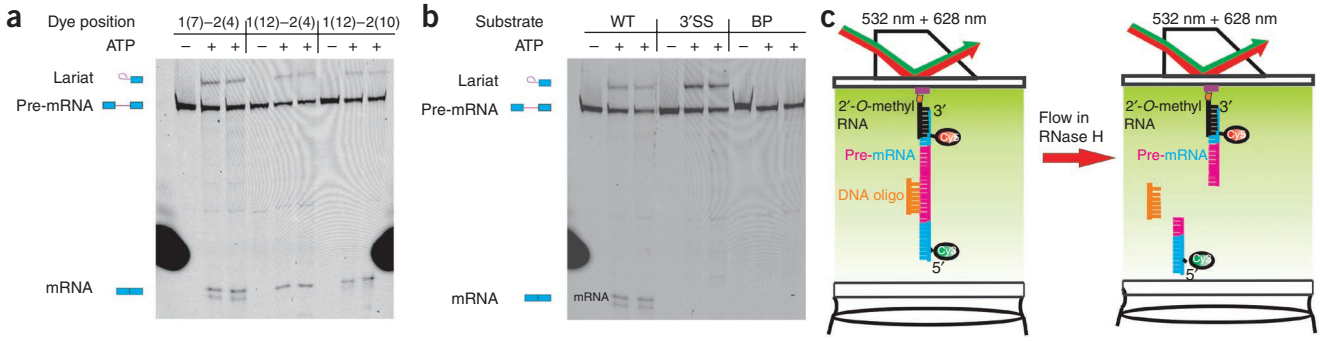

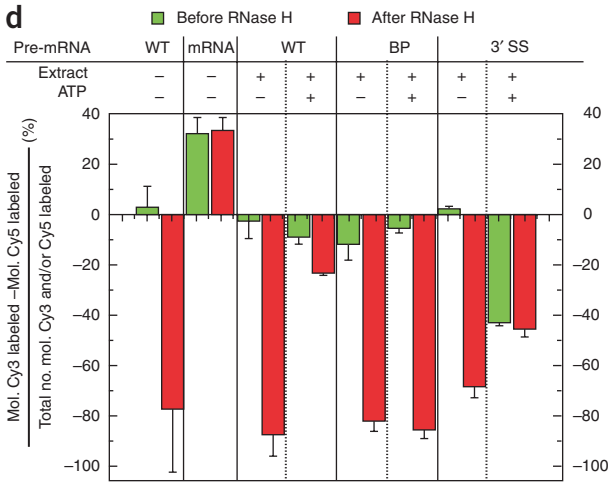

Figure 2 Splicing activity of different Ubc4 pre-mRNA variants. (**a**) Positioning the dyes in different sites in the 20-nt exon of Ubc4 pre-mRNA results in similar splicing efficiency. In this experiment, splicing was assayed at room temperature as described in Online Methods. The three lanes for each pre-mRNA from left to right are –ATP, +ATP for 15 min and +ATP for 30 min. All pre-mRNAs examined have an apparent splicing efficiency of first plus second step ([mRNA + lariat intermediate] / [pre-mRNA + mRNA + lariat intermediate]) of 30–40%. The Cy5 fluorescence scan is shown. (**b**) The splicing assay of WT, 3′SS and BP Ubc4 pre-mRNA shows that the 3′SS mutant RNA only carries out step 1, leading to a lariat-intron intermediate. The BP mutant is inactive in splicing. The experiment was carried out as described for **a**. The Cy5 fluorescence scan is shown. (**c**) Design of an *in situ* assay to probe for the presence of introns in immobilized (pre-) mRNAs. (**d**) Results of RNase H probing for the presence of the intron after incubation of WT, BP and 3′SS pre-mRNA in yeast splicing extract. Control experiments on WT pre-mRNA and mature mRNA (leftmost four columns) show that an intron containing substrate strongly loses Cy3 signal after incubation with a complementary DNA oligonucleotide and RNase H but not the intron-free mRNA. Loss of the intron to splicing is thus indicated by a small difference in signal before and after RNase H treatment. Error bars, ± 1 s.d. from the mean.

immobilized and incubated in either ATP-depleted (–ATP) or ATP-supplemented (+ATP) yeast splicing extract for 1 h (Online Methods and **Fig. 2c**). Only pre-mRNA was expected and experimentally found to be susceptible to RNase H degradation, leading to the specific loss of the 5′ exon and thus Cy3 signal from the slide surface, whereas the mature mRNA was resistant to RNase H (first four columns of **Fig. 2d**). We found that after incubation in –ATP cell extract, 75% of all molecules lost Cy3 but not Cy5 upon RNase H challenge, whereas in +ATP this fraction was negligible (**Fig. 2d**). Performing the same assay with the BP mutant results in extensive loss of Cy3 signal upon addition of RNase H both before and after incubation in +ATP extract (**Fig. 2d**), consistent with the expected block of the first step of splicing. The 3′SS mutant showed an intermediate picture, as much of its Cy3 signal was lost during the high-salt washes used to remove the cell extract (**Fig. 2d**), consistent with a block after the first step of splicing, when the 5′ exon is no longer covalently attached to the intron. These results support the notion that the immobilized WT pre-mRNA is splicing active to at least the extent observed in standard ensemble splicing assays in solution (~30–40%, see above). The apparent increase in splicing efficiency of the immobilized WT substrate may be the result of the more favorable stoichiometric ratio of limiting splicing factors to pre-mRNA under our single-molecule conditions. Additionally, effects such as RNA aggregation and precipitation are known to inhibit reactions under

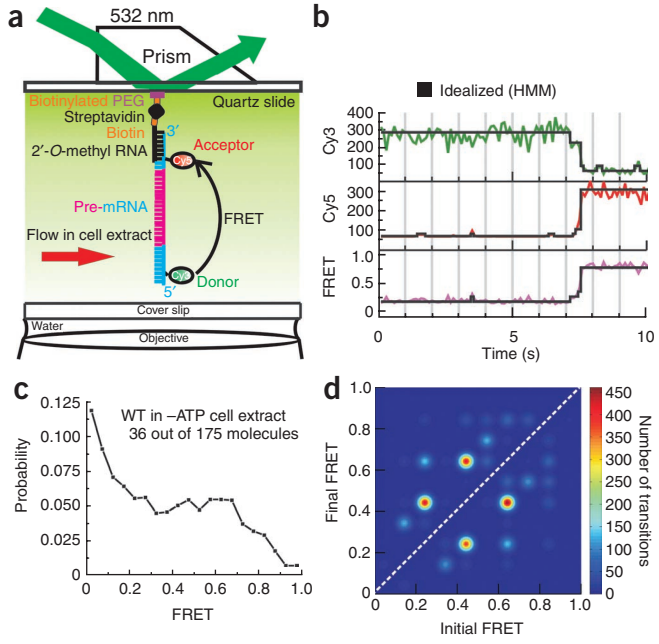

Figure 3 Data analysis and examples of analysis. (**a**) Synthetic Ubc4 pre-mRNA is hybridized via a 17-nt 2′-*O*-methyl RNA tether to the 3′ exon and attached via biotin to a streptavidin-coated quartz slide. (**b**) Raw Cy3 (green), Cy5 (red) and FRET (magenta) time trajectories are analyzed using HMM algorithms to yield idealized trajectories (black) as described in the Online Methods. (**c**) The first 10 s of the raw FRET trajectories of a subset (36 out of 175) of WT molecules incubated in ATP-depleted (–ATP) cell extract were analyzed to determine the ensemble distribution of FRET states within the population of molecules analyzed. (**d**) TDPs use the idealized FRET trajectories to determine the entire set of transitions for a given set of molecules. The number of times a transition occurs is represented as a heat map whose index is defined by the color bar. The fact that this analysis of a subset (36 of 175 molecules, as in **c**) of the data shown in **Figures 5a** and **6a** provides qualitatively the same result obtained for the full dataset attests to the convergence of the analysis.

in vitro conditions that favor intramolecular (and thus, inevitably, intermolecular) interactions[22]. Immobilization of isolated pre-mRNAs for single-molecule studies is expected to suppress such inhibition and may thus provide ideal conditions for studying splicing.

Dissecting conformational states and dynamics

Our smFRET approach monitors the relative dynamic positioning of the two exons within the spliceosomal complex. Results are presented in three ways. First, we show smFRET time trajectories with their corresponding donor and acceptor traces, which reveal multiple discrete FRET values or states that reflect the complexity of pre-mRNA conformational rearrangements during spliceosome assembly (**Fig. 3b**). Second, FRET-occupancy histograms show the probability of observing a particular FRET value (**Fig. 3c**). In these histograms, we plot frame-by-frame FRET values for a set of molecules collected over the first 100 frames (10 s of real time) of all FRET trajectories in a given dataset, which is proportional to the probability that any single molecule will have that FRET value.

Third, we used traditional transition density plots (TDPs), weighted by the number of times a particular FRET transition occurs, as well as novel population-weighted and kinetically indexed transition density (POKIT) plots, which we developed for this study, to comprehensively represent all observed discrete FRET states, their transitions and their kinetics. To first reliably identify genuine FRET states and their transition kinetics in naturally noisy datasets, we used hidden Markov modeling (HMM), which traces the most probable sequence of FRET states and derives their dwell times[23] (Online Methods and **Fig. 3b**). To eliminate from our analysis possible effects of the high concentrations of proteins directly on the fluorophores, we evaluated the donor and acceptor signals by HMM and introduced a scoring function selecting for anticorrelated donor and acceptor changes that reflect changes in FRET (see Online Methods and **Supplementary Fig. 2**). As a further control, we monitored the donor and acceptor signals from a mature (synthetic) mRNA under the same conditions used for the pre-mRNA and found a largely steady FRET signal (**Supplementary Fig. 3**). These observations indicate that any smFRET dynamics we

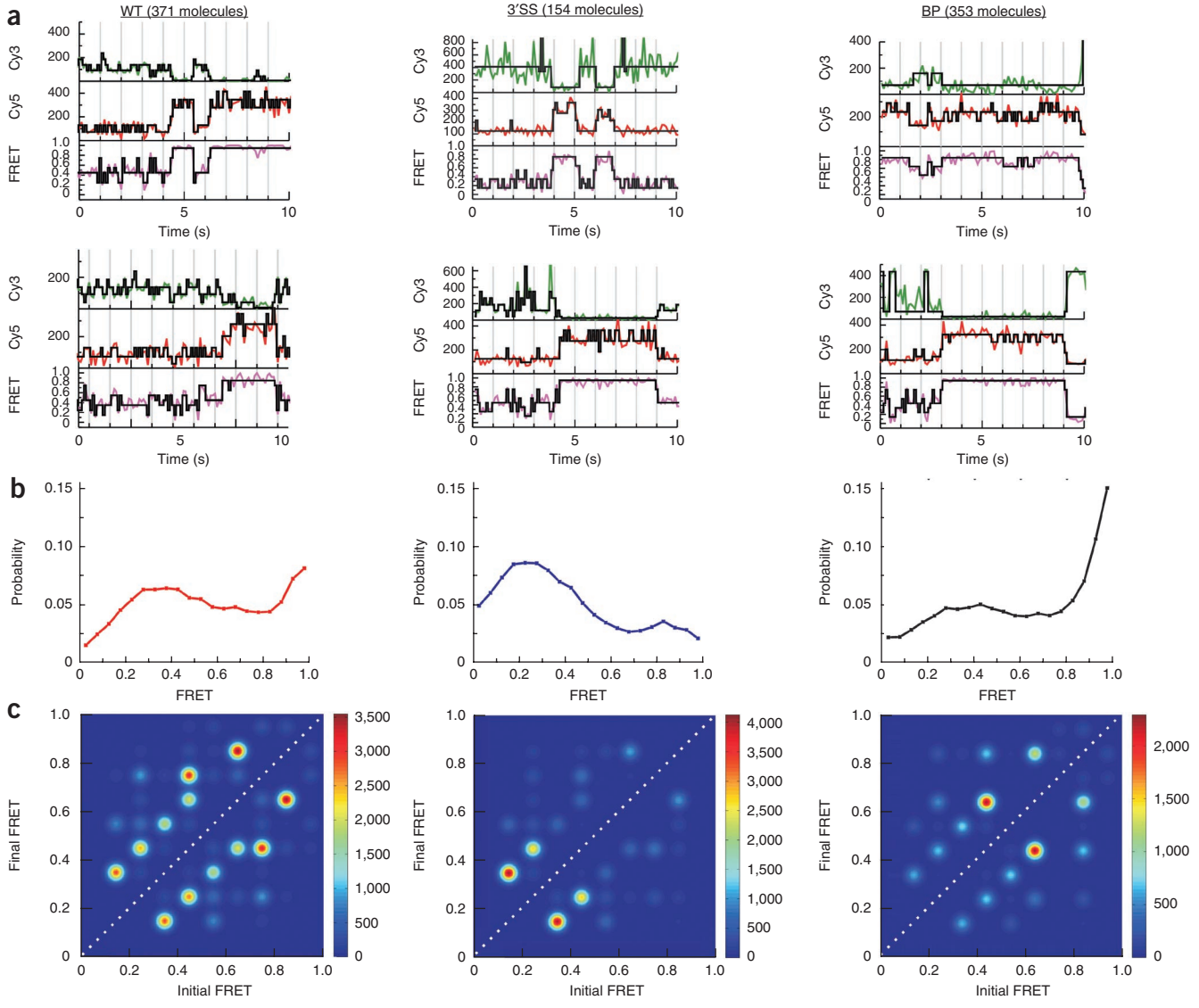

Figure 4 Conformational dynamics of WT, 3′SS and BP pre-mRNA substrates in splicing buffer. (**a**) Sample traces of all three substrates in splicing buffer, showing raw donor (Cy3, green), acceptor (Cy5, red) and FRET (blue) trajectories and their idealized HMM models (black). (**b**) FRET histograms of the three pre-mRNAs in splicing buffer. (**c**) TDPs for all three pre-mRNAs in splicing buffer.

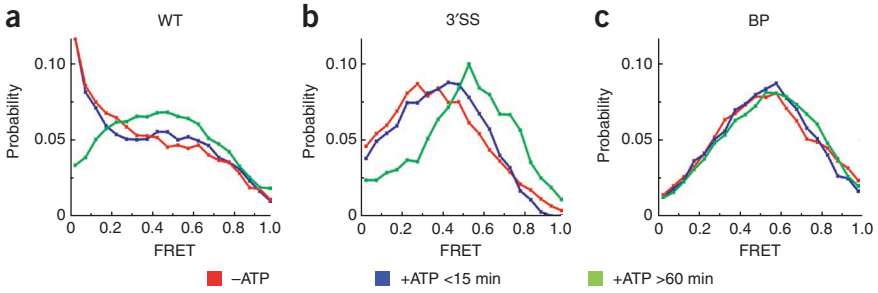

Figure 5 ATP-dependent conformational dynamics of the WT, 3′SS and BP pre-mRNAs in yeast cell extract. (**a**–**c**) Probability distributions of FRET states for WT (**a**), 3′SS (**b**) and BP (**c**) substrates for each experimental condition.

observed for pre-mRNA were not caused by spurious photophysical artifacts but by the expected changes in fluorophore distance.

To determine the most likely number of states in our smFRET trajectories, we analyzed whole datasets of 50–200 single-molecule traces by our scored HMM approach. The best global fit to the entire trace set for each condition generally found 10 or 11 distinct FRET states (to be evaluated as distinct, two states needed to show a FRET difference of at least 0.1; see Online Methods), with each molecule adopting only a subset of states (**Supplementary Fig. 4**). With knowledge of the number of states in each dataset, we identified the transitions between these states, summarized as TDPs[24] and POKIT plots (**Supplementary Fig. 5**). The transition from an initial FRET state of 0.8, for example, to a final FRET state of 0.3 is one point in these plots. There can be a maximum of $n(n-1)$ different transitions between n states. We observed many fewer than the 110 possible transitions.

To test the robustness of our analysis, we randomly selected a subset of 36 out of a total of 175 WT substrate molecules in –ATP extract and found that this subset yielded a similar FRET-occupancy histogram and TDP as the entire dataset (**Fig. 3c**,**d**), suggesting that our molecule sample is of sufficient size for the HMM model to converge.

Pre-mRNA dynamically folds and unfolds in splicing buffer

When incubated in standard splicing buffer alone, all three pre-mRNAs showed substantial global dynamics with fluctuations between high- and low-FRET states (**Fig. 4a**). The several-second-long dwell times in high-FRET states indicate that the pre-mRNAs must transiently form secondary structures that bring the distal 5′ and 3′ splice sites into close proximity. The distribution of FRET states is not identical between the pre-mRNAs, as WT and BP favor high-FRET states (shorter distances) relative to 3′SS. By comparison, 3′SS spends relatively more time in low-FRET states, as is evident from the cumulative FRET-occupancy histograms (**Fig. 4b**). These differences are also apparent in the corresponding TDPs, where the WT and BP pre-mRNAs show more transitions in the high-FRET (>0.7) and fewer in the low-FRET (<0.4) range than does 3′SS. Notably, there are some transitions with long dwell times found in all pre-mRNAs (**Fig. 4a**,**c**). Computational predictions suggest that in the ensembles of lowest free-energy states, distinct secondary structures separate the 5′ and 3′ splice sites in WT and BP less than in 3′SS, qualitatively correlating with their experimentally observed relative bias toward higher FRET values (**Supplementary Fig. 6**).

All RNA molecules assume transient secondary structures[25], so it is not surprising that the Ubc4 pre-mRNA shows transient folding yielding high-FRET states. In the case of Ubc4 pre-mRNA, even single base changes affect these structures. That we can observe these single base differences by smFRET attests to the power of this method. Furthermore, this kinetic analysis of the substrate RNA in buffer is necessary to distinguish the pre-mRNA dynamics caused by the formation of transient secondary structures from those induced by spliceosome assembly. To achieve a maximal dynamic time range for observing spliceosome related kinetics, in the following we performed 100-ms time resolution smFRET experiments at various instances after addition of splicing extract.

Dynamics of single pre-mRNAs in splicing extract

The addition of –ATP yeast splicing extract resulted in a profound difference from the FRET histograms observed in buffer alone (compare **Figs. 4b** and **5**). Lower FRET values were relatively favored for all three pre-mRNAs. The effect is most pronounced for WT, which became biased toward particularly low-FRET values. These changes to lower FRET distributions show that the relatively stable high-FRET states observed in buffer alone are disfavored in extract.

The addition of ATP to extract (+ATP) led to a time-dependent change in the FRET distributions of the WT and 3′SS pre-mRNAs but not that of BP (**Fig. 5**). In the case of 3′SS, the overall FRET distribution changed within 15 min and after 60 min of incubation in +ATP extract to increasingly more prevalent mid- and high-FRET

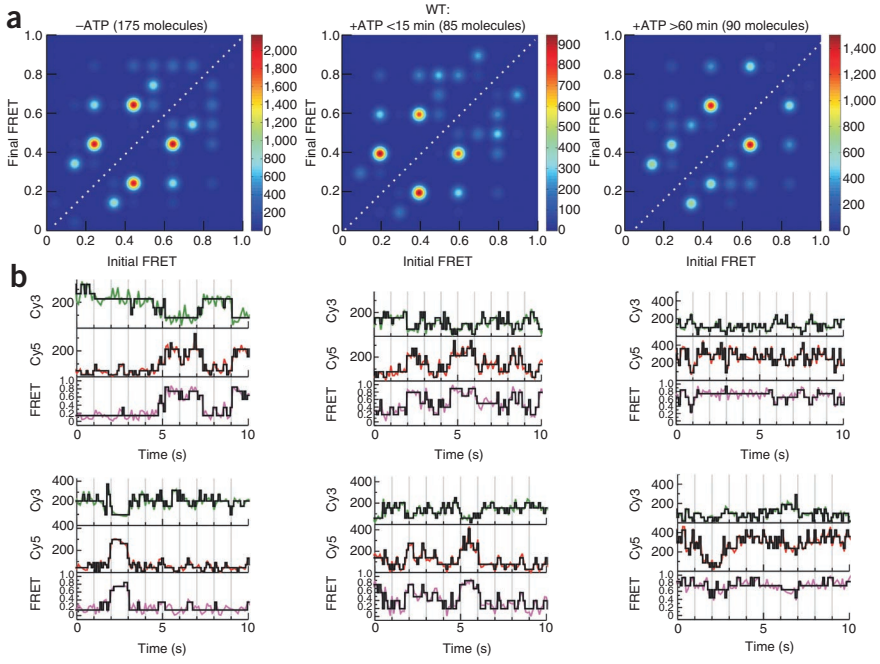

Figure 6 Mapping conformational changes of the WT pre-mRNA during spliceosome assembly and splicing *in vitro*. (**a**) TDPs for WT substrate in ATP-depleted extract (–ATP), within 15 min after ATP addition to cell extract (+ATP <15 min) and after 60 min incubation in +ATP cell extract (+ATP >60 min). (**b**) Representative trajectories (donor, green; acceptor, red; FRET, magenta) and idealized HMM models (black) for WT substrate.

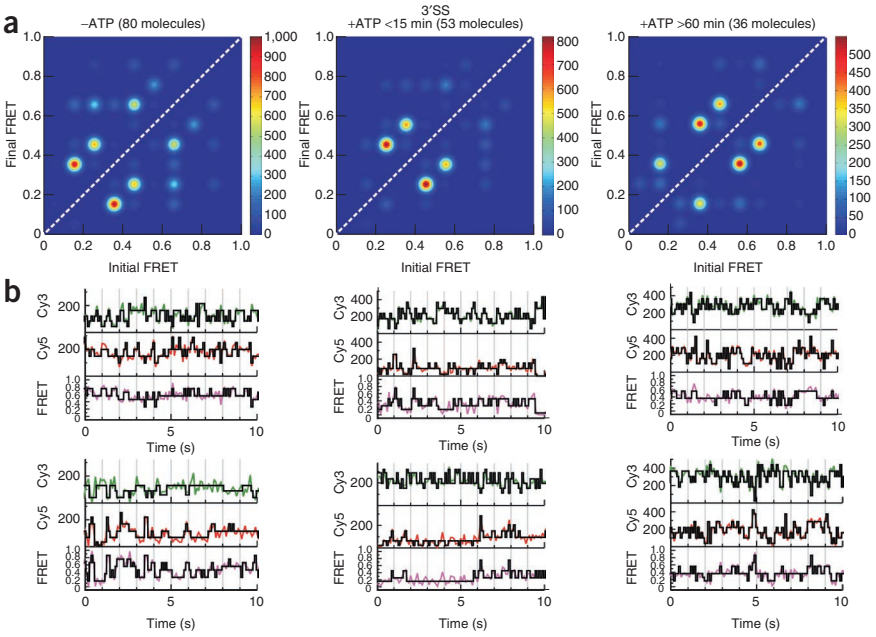

Figure 7 Mapping conformational changes of the 3′SS pre-mRNA spliceosome assembly and splicing *in vitro*. (**a**) TDPs for 3′SS substrate in ATP-depleted extract (–ATP), within 15 min after ATP addition to cell extract (+ATP <15 min) and after 60 min incubation in +ATP cell extract (+ATP >60 min). (**b**) Representative trajectories (donor, green; acceptor, red; FRET, magenta) and idealized HMM models (black) for 3′SS substrate.

states (**Fig. 5b**). In the case of WT, the prevalent low-FRET states were lost over 60 min of incubation (**Fig. 5a**), whereas BP showed no substantial change in the overall FRET distribution (**Fig. 5c**), in agreement with the requirement of an intact branchpoint for ATP-dependent spliceosome assembly[17]. Thus, the time-dependent changes in FRET distribution upon addition of ATP require a pre-mRNA substrate that can undergo the first step (3′SS) or both steps (WT) of splicing.

The time-, ATP- and mutation-dependent changes in the FRET histograms observed upon incubation in extract suggest that we are observing splicing-dependent changes at the single-molecule level, but FRET histograms cannot tell us about the dynamics of those changes. To track even subtle changes in these conformational dynamics upon addition of splicing extract, we turned to HMM and TDP analysis.

Spliceosome dependent dynamics of pre-mRNA substrates

The TDP of WT pre-mRNA shows that, upon addition of –ATP cell extract, fewer transitions were observed than were seen for the same substrate in buffer, and the most prevalent transitions were on average lower on the FRET scale (compare **Figs. 4c** and **6a**). Within the first 15 min after the addition of +ATP cell extract, the distribution of transitions changed yet again, with more transitions originating from the 0.8 FRET state. After a 60-min incubation in +ATP cell extract, FRET transitions appeared in an even higher-FRET region (0.75–0.95), indicating that conformations are favored where the two exons are in close proximity (**Fig. 6a**). Most observed FRET transitions are reversible, leading to the relative mirror symmetry of the TDPs with respect to their main diagonal (**Fig. 6a**). Reversible FRET transitions imply conformational reversibility, a property that is characteristic of all substrates and extract conditions (**Figs. 6–8** and **Supplementary Fig. 7**).

Upon addition of –ATP extract, the 3′SS pre-mRNA, like the WT, showed fewer, still symmetric (in other words, reversible) transitions than in buffer (compare **Figs. 4c** and **7a**). After a 15-min incubation in +ATP cell extract (compare **Figs. 6** and **7**), there was a shift toward higher-FRET states. Most notably, transitions that became more prevalent after a 60-min incubation in +ATP extract generally fell into a mid-FRET regime (**Fig. 7a**), unlike for WT, for which a shift occurred toward high-FRET transitions (**Fig. 6a**).

The BP mutant does not enter the spliceosome assembly pathway (**Fig. 1**), and despite our observation of transitions between a substantial number of FRET states (and unlike with the WT and 3′ SS substrates), we observed few changes for BP when comparing the FRET states in –ATP extract and +ATP extract. The prominent set of symmetric transitions between 0.45 and 0.65 FRET were present before and after the addition of +ATP extract (**Fig. 8a–c**). After 60 min in +ATP extract, the number and diversity of transitions sampled by each BP molecule was only slightly changed.

To assess the kinetic differences between substrates, we turned to POKIT plot analysis.

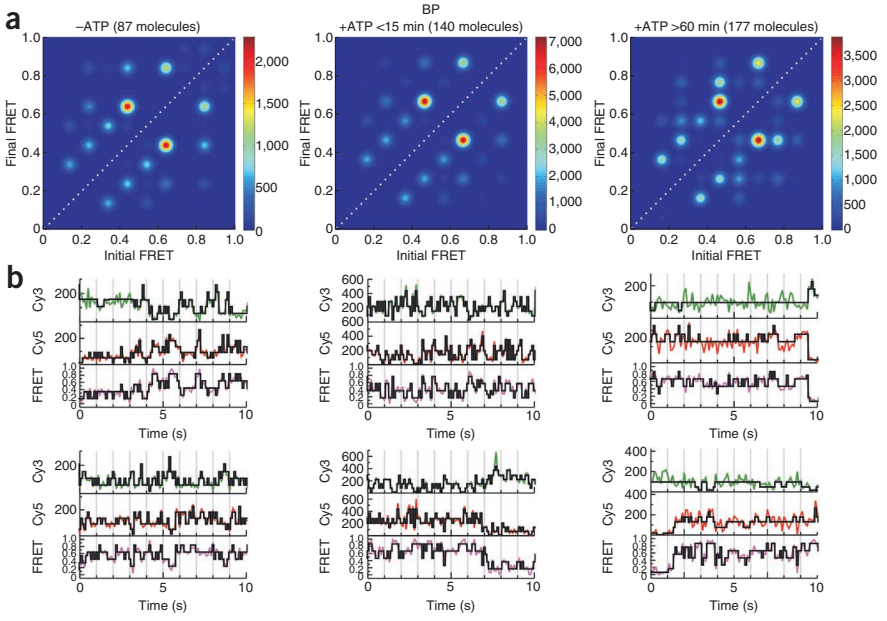

Figure 8 Mapping conformational changes of the BP pre-mRNA spliceosome assembly and splicing *in vitro*. (**a**) TDPs for BP substrate in ATP-depleted extract (–ATP), within 15 min after ATP addition to cell extract (+ATP <15 min) and after 60 min incubation in +ATP cell extract (+ATP >60 min). (**b**) Representative trajectories (donor, green; acceptor, red; FRET, magenta) and idealized HMM models (black) for BP substrate.

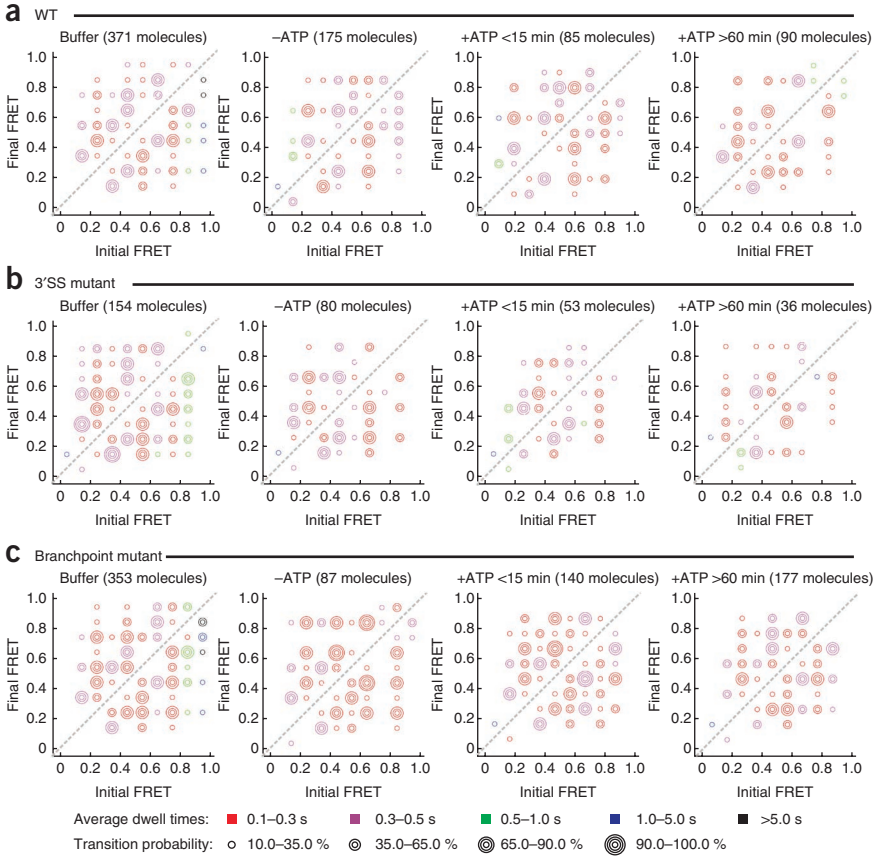

Figure 9 Detailed comparison of kinetic and conformational profiles of pre-mRNAs during spliceosome assembly and splicing *in vitro*. (**a**–**c**) POKIT plots for WT (**a**), 3′SS (**b**) and BP (**c**) substrates in ATP-depleted extract (–ATP), within 15 min after ATP addition to cell extract (+ATP <15 min) and after 60 min incubation in +ATP cell extract (+ATP >60 min).

Supplementary Figure 5 provides a side-by-side comparison of these plots with the more common TDPs to illustrate their close relationship; however, POKIT plots provide two additional, comprehensive pieces of information for each transition. First, they present as a number of concentric circles the fraction of molecules in the entire trace set that shows a specific FRET transition at least once (**Supplementary Fig. 5**). This feature complements TDPs that are weighted by the number of times a specific transition is observed overall[24], which emphasizes fast (frequent) transitions shown by possibly only a small fraction of molecules (**Supplementary Fig. 5**). Second, our POKIT plots provide the average dwell time for each transition, or time spent in the initial state before transition to the final state, in the form of circle colors (**Supplementary Fig. 5**), facilitating the rapid visual comparison of the kinetics of our various smFRET datasets as a function of ATP concentration, incubation time and intron signals.

The POKIT plots of the WT pre-mRNA in buffer and in –ATP extract highlight the fact that incubation with cell extract induced longer dwell times in low- rather than high-FRET states (**Fig. 9**). Within the first 15 min after the addition of +ATP cell extract, the distribution of transitions then changed to include a higher fraction of molecules with FRET transitions in the 0.6–0.9 range (**Fig. 9**). After a 60-min incubation in +ATP cell extract, this trend continued toward even longer dwell times in an even higher-FRET region (0.75–0.95, **Fig. 9**), indicating that relatively stable conformations are favored where the two exons are proximal. We observed these long dwell times in the highest-FRET states only for the WT substrate, and they required an extended incubation with +ATP cell extract (**Fig. 9**). The fact that similar transitions were strongly dominant for the mature (synthetic) mRNA control (**Supplementary Fig. 3**) but were found in only ~20% of all WT molecules (**Fig. 9**) suggests that only a fraction of the total WT pre-mRNA observed after 60 min in +ATP cell extract adopted a conformation similar to that of the synthetic mRNA. These findings indicate that most pre-mRNA molecules are spliced reversibly, possibly because our 2′-*O*-methyl RNA tether hybridized to the short 3′ exon blocks the binding of the pre-mRNA splicing factor Prp22 and disrupts spliceosome disassembly[25]; alternatively (or additionally), these findings may indicate that the mRNA derived from the activity of bound splicing factors has a FRET signature distinct from that of the synthetic mRNA, which is not expected to bind splicing factors.

In summary, our data suggest that, *in vitro*, the WT pre-mRNA samples both low- and high-FRET conformational states, even in the absence of splicing extract. The addition of extract leads to a change in the distribution and kinetics of these FRET states, first through the assembly of spliceosomal components on the pre-mRNA in the absence of ATP and, second, by extended incubation with ATP-enriched cell extract over a time period where the pre-mRNA undergoes both steps of splicing (**Fig. 2**). Additionally, after 60 min in splicing extract, WT pre-mRNA adopts relatively stable high-FRET conformations that are also found in an mRNA control, but not in mutant substrates, placed under the same conditions (**Figs. 6–9** and **Supplementary Fig. 3**). The BP mutant largely lacks these time- and ATP-dependent changes, whereas the 3′SS mutant is generally more similar to the WT than the BP mutant but does not achieve the stable high-FRET states after a 60-min incubation that are observed for the WT substrate. Most conformational changes of the pre-mRNAs are readily reversible, and their relative abundance and kinetics are both dependent on both ATP and intron signals, implying that these changes are relevant for splicing activity.

DISCUSSION

Establishment of smFRET to monitor spliceosome assembly

In this study, we used smFRET to observe the conformational dynamics of a pre-mRNA during spliceosome assembly. We identified Ubc4 as a natural intron-containing transcript that is both small—allowing ease of chemical synthesis—and very efficiently spliced *in vitro* as well as *in situ* during our smFRET experiments (**Fig. 2**). We placed the donor fluorophore Cy3 in exon 1 near the 5′ splice site and the acceptor Cy5 in exon 2 near the 3′ splice site. With this substrate under standard *in vitro* splicing conditions, we observed a splicing efficiency of 30–40%, which *in situ* may be even higher (**Fig. 2**). This result is not unique to the Ubc4 substrate; recent work showed that a different fluorescently labeled pre-mRNA bound to a slide for TIRFM studies undergoes splicing (measured as the release of a fluorescent intron) upon addition of splicing extract[26]. The authors did not, however, monitor the structural dynamics of the pre-mRNA during spliceosome assembly and action as we have done here.

Several criteria establish that the smFRET changes we observed in splicing extract reflect dynamic changes in the substrate during spliceosome assembly. These criteria are that the dynamic changes should be time and ATP dependent and that they should be affected as expected by mutations in the substrate. The FRET-occupancy histograms (**Fig. 5**) show that we indeed observed time- and ATP-dependent changes for the WT substrate and the 3′SS mutant but, as expected, less so for the BP mutant (see also below). These results show that we monitored conformational changes associated with genuine spliceosome assembly processes.

Conformational dynamics are altered by intron mutations

When −ATP extract was added, we observed substantial differences in FRET histograms and FRET transitions of all three pre-mRNAs. More specifically, the smFRET transitions observed in splicing buffer alone were replaced by a somewhat smaller set of transitions with on-average shorter dwell times (**Figs. 4** and **6–9**). This initial shift in FRET distribution of all pre-mRNAs upon extract addition is consistent with the presence of a large number of highly concentrated RNA binding proteins in yeast extract—for example, the RNP protein NPL3 (ref. 27). These proteins are expected to alter transient secondary structures, but they are not expected to distinguish between RNA molecules differing by a single base change. Notably, the WT adopted a set of low-FRET conformations with slow transitions that are not found in the 3′SS and BP mutants. As is evident from **Figure 1**, the behavior of WT may reflect the ATP-independent interaction of the U1 snRNP with the 5′ splice site, branchpoint binding protein (SF1 in humans) and Mud2 (U2AF in mammals) with the branchpoint and polypyrimidine tract to form the commitment complex. In any event, because an intact branchpoint is required for the resistance of a labeled pre-mRNA template to challenge by excess cold substrate[28], we predicted that the BP mutant would be blocked at the earliest stage of spliceosome assembly. This is fully consistent with our observation of substantial differences in the TDP and POKIT patterns of WT and 3′SS mutant on the one hand and BP mutant on the other (**Figs. 6–9**).

The 3′SS mutant was predicted to largely mimic the WT pattern, given that the 3′SS sequence is thought to be required only for the second chemical step. This prediction is consistent with the greater similarity of the TDP and POKIT plots of the WT and 3′SS mutant compared to those of the BP mutant. Curiously, the 3′SS mutant, unlike WT, does not adopt stable low-FRET transitions in the absence of ATP (**Fig. 9**). These stable transitions appear in the 3′SS mutant only after addition of +ATP extract, and they are never observed in the BP mutant. It is tempting to speculate that our detailed kinetic smFRET analysis reveals differences between WT and 3′SS that are not detectable by conventional assays. Other discrepancies in the canonical model of spliceosome assembly (**Fig. 1**) have been noted previously, and the list of these will likely expand with the emergence of new experimental tools[29,30].

The spliceosome, like the ribosome, functions near equilibrium

As described in the introduction, a dominant and well-known feature of splicing is the highly dynamic nature of the spliceosome, which in yeast is driven forward by eight RNA-dependent ATPases of the DEAD-box family[2]. It is thought that each of the eight DEAD-box–dependent steps in splicing provide fidelity checkpoints[6,7]. Evidence for this model is found in our observation that, within the first 15 min of incubation of WT pre-mRNA in ATP-enriched extract, the molecule population shifted toward higher-FRET transitions compared to the transitions in ATP-depleted extract (**Figs. 6** and **9**). This indicates that the assembly and rearrangements of spliceosomal components initiated by ATP bring the two exons closer to each other, as envisioned in the model to achieve splicing-specific conformations. The effect is more pronounced after a long incubation (60 min) with ATP-enriched extract (**Figs. 6** and **9**), when a substantial fraction of mRNA product has been generated (**Fig. 2**).

Historically, it has been assumed that the spliceosomal ATPases would drive the pathway unidirectionally. Our observation of the dynamics of single pre-mRNAs indicates that the substrate does not follow a simple unidirectional pathway. Instead, pre-mRNAs sample a variety of reversible conformational states guided by the assembly of ATP-dependent spliceosomal components. Recently, it has been shown that the chemical steps are themselves reversible, at least under certain *in vitro* conditions[31,32]. A reversal of the chemical steps of splicing requires that the conformation of the substrate and spliceosome assembly be reversible as well. Such a model is supported by our observation of reversible smFRET transitions. To our knowledge, our data provide the first direct glimpse of such reversible conformational changes of the pre-mRNA throughout the splicing process. This realization prompts a provocative re-evaluation of the role of ATP in splicing, in which the function of hydrolysis is largely to improve the accuracy of the pathway, driving the 'correct' substrate to completion and rejecting 'incorrect' alternatives. Notably, this picture fits well with recent evidence from the ribosome, in which spontaneous intersubunit rotation has been observed in the absence of GTP[33]. Thus it is tempting to speculate that both macromolecular machines carry out complex sets of conformational changes close to thermal equilibrium.

Outlook

We have shown that, during spliceosome assembly, a pre-mRNA's conformations are highly dynamic and largely reversibly interchanging. These changes are reflected in a large number of complex transitions. By locating the dyes at different pre-mRNA positions, by placing the dyes in snRNAs or proteins and by examining the effects of mutant extracts, it now seems possible to assign particular sets of FRET transitions to specific steps in spliceosome assembly. Ultimately, approaches such as these will yield a comprehensive dynamic model of pre-mRNA splicing.

METHODS

Methods and any associated references are available in the online version of the paper at http://www.nature.com/nsmb/.

Note: Supplementary information is available on the Nature Structural & Molecular Biology website.

ACKNOWLEDGMENTS

The authors wish to thank R. Lührmann and P. Fabrizio (Max Planck Institute for Biophysical Chemistry), J. Staley (Univ. Chicago) and B. Schwer (Weill Cornell Medical College) for providing splicing active yeast cell extracts at a moment, common in this field, in which we were having difficulty in making active extracts, as well as G. Whitworth, J. Staley and H. Hadjivassiliou for helpful comments on the manuscript. The oligonucleotides synthesized at Dharmacon were sometimes much longer than those they usually make, and their excellent quality was essential for this project. The work at the University of Michigan was supported by US National Institutes of Health (NIH) grant GM062357 to N.G.W. and NIH Cellular & Molecular Biology and Molecular Biophysics Training Grant fellowships to M.B. and M.A.D., respectively, as well as a Rackham Merit Fellowship to M.B. The work at the University of California, San Francisco (UCSF), was supported by an American Cancer Society Research Professor of Molecular Genetics award to C.G., by NIH grant GM021119 to C.G., by NIH postdoctoral fellowship GM077844 to C.M. and by a grant from the Agouron Institute to J.A.

AUTHOR CONTRIBUTIONS

J.A. worked at the bench and led the development of the Ubc4 system at UCSF; J.A.P. and J.A. performed the microarray analysis in **Supplementary Table 1**; D.E.R.,

T.V. and C.M. participated in various phases of the biochemistry at UCSF; M.B., M.A.D., F.F. and M.W. performed the smFRET experimentation and data analysis; P.A. performed the secondary structure analysis at the University of Michigan; J.A., M.A.D., M.B., C.M., C.G. and N.G.W. wrote the manuscript.

COMPETING FINANCIAL INTERESTS

The authors declare no competing financial interests.

Published online at http://www.nature.com/nsmb/.
Reprints and permissions information is available online at http://npg.nature.com/reprintsandpermissions/.

1. Jurica, M.S. & Moore, M.J. Pre-mRNA splicing: awash in a sea of proteins. *Mol. Cell* **12**, 5–14 (2003).
2. Wahl, M.C., Will, C.L. & Luhrmann, R. The spliceosome: design principles of a dynamic RNP machine. *Cell* **136**, 701–718 (2009).
3. Staley, J.P. & Guthrie, C. Mechanical devices of the spliceosome: motors, clocks, springs, and things. *Cell* **92**, 315–326 (1998).
4. Burgess, S.M. & Guthrie, C. A mechanism to enhance mRNA splicing fidelity: the RNA-dependent ATPase Prp16 governs usage of a discard pathway for aberrant lariat intermediates. *Cell* **73**, 1377–1391 (1993).
5. Couto, J.R., Tamm, J., Parker, R. & Guthrie, C. A *trans*-acting suppressor restores splicing of a yeast intron with a branch point mutation. *Genes Dev.* **1**, 445–455 (1987).
6. Mayas, R.M., Maita, H. & Staley, J.P. Exon ligation is proofread by the DExD/H-box ATPase Prp22p. *Nat. Struct. Mol. Biol.* **13**, 482–490 (2006).
7. Xu, Y.Z. & Query, C.C. Competition between the ATPase Prp5 and branch region–U2 snRNA pairing modulates the fidelity of spliceosome assembly. *Mol. Cell* **28**, 838–849 (2007).
8. Walter, N.G., Huang, C.Y., Manzo, A.J. & Sobhy, M.A. Do-it-yourself guide: how to use the modern single-molecule toolkit. *Nat. Methods* **5**, 475–489 (2008).
9. Furman, E. & Glitz, D.G. Purification of the spliceosome A-complex and its visualization by electron microscopy. *J. Biol. Chem.* **270**, 15515–15522 (1995).
10. Jurica, M.S., Licklider, L.J., Gygi, S.R., Grigorieff, N. & Moore, M.J. Purification and characterization of native spliceosomes suitable for three-dimensional structural analysis. *RNA* **8**, 426–439 (2002).
11. Kent, O.A. & MacMillan, A.M. Early organization of pre-mRNA during spliceosome assembly. *Nat. Struct. Biol.* **9**, 576–581 (2002).
12. Newman, A.J., Teigelkamp, S. & Beggs, J.D. snRNA interactions at 5′ and 3′ splice sites monitored by photoactivated crosslinking in yeast spliceosomes. *RNA* **1**, 968–980 (1995).
13. Lin, R.J., Newman, A.J., Cheng, S.C. & Abelson, J. Yeast mRNA splicing *in vitro*. *J. Biol. Chem.* **260**, 14780–14792 (1985).
14. Vijayraghavan, U., Company, M. & Abelson, J. Isolation and characterization of pre–mRNA splicing mutants of *Saccharomyces cerevisiae*. *Genes Dev.* **3**, 1206–1216 (1989).
15. Clark, T.A., Sugnet, C.W. & Ares, M. Jr. Genomewide analysis of mRNA processing in yeast using splicing-specific microarrays. *Science* **296**, 907–910 (2002).
16. Pleiss, J.A., Whitworth, G.B., Bergkessel, M. & Guthrie, C. Transcript specificity in yeast pre-mRNA splicing revealed by mutations in core spliceosomal components. *PLoS Biol.* **5**, e90 (2007).
17. Vijayraghavan, U. *et al.* Mutations in conserved intron sequences affect multiple steps in the yeast splicing pathway, particularly assembly of the spliceosome. *EMBO J.* **5**, 1683–1695 (1986).
18. Rueda, D. *et al.* Single-molecule enzymology of RNA: essential functional groups impact catalysis from a distance. *Proc. Natl. Acad. Sci. USA* **101**, 10066–10071 (2004).
19. Ditzler, M.A., Rueda, D., Mo, J., Hakansson, K. & Walter, N.G. A rugged free energy landscape separates multiple functional RNA folds throughout denaturation. *Nucleic Acids Res.* **36**, 7088–7099 (2008).
20. Pereira, M.J. *et al.* Single vs. ribozyme molecules reveal dynamic and hierarchical folding toward catalysis. *J. Mol. Biol.* **382**, 496–509 (2008).
21. de Silva, C. & Walter, N.G. Leakage and slow allostery limit performance of single drug-sensing aptazyme molecules based on the hammerhead ribozyme. *RNA* **15**, 76–84 (2009).
22. Bartel, D.P. & Szostak, J.W. Isolation of new ribozymes from a large pool of random sequences. *Science* **261**, 1411–1418 (1993).
23. Munro, J.B., Altman, R.B., O'Connor, N. & Blanchard, S.C. Identification of two distinct hybrid state intermediates on the ribosome. *Mol. Cell* **25**, 505–517 (2007).
24. McKinney, S.A., Joo, C. & Ha, T. Analysis of single-molecule FRET trajectories using hidden Markov modeling. *Biophys. J.* **91**, 1941–1951 (2006).
25. Schwer, B. A conformational rearrangement in the spliceosome sets the stage for Prp22-dependent mRNA release. *Mol. Cell* **30**, 743–754 (2008).
26. Crawford, D.J., Hoskins, A.A., Friedman, L.J., Gelles, J. & Moore, M.J. Visualizing the splicing of single pre-mRNA molecules in whole cell extract. *RNA* **14**, 170–179 (2008).
27. Ghaemmaghami, S. *et al.* Global analysis of protein expression in yeast. *Nature* **425**, 737–741 (2003).
28. Seraphin, B. & Rosbash, M. Identification of functional U1 snRNA–pre-mRNA complexes committed to spliceosome assembly and splicing. *Cell* **59**, 349–358 (1989).
29. Stevens, S.W. *et al.* Composition and functional characterization of the yeast spliceosomal penta-snRNP. *Mol. Cell* **9**, 31–44 (2002).
30. Maroney, P.A., Romfo, C.M. & Nilsen, T.W. Functional recognition of 5′ splice site by U4/U6.U5 tri-snRNP defines a novel ATP-dependent step in early spliceosome assembly. *Mol. Cell* **6**, 317–328 (2000).
31. Smith, D.J. & Konarska, M.M. Mechanistic insights from reversible splicing catalysis. *RNA* **14**, 1975–1978 (2008).
32. Tseng, C.K. & Cheng, S.C. Both catalytic steps of nuclear pre-mRNA splicing are reversible. *Science* **320**, 1782–1784 (2008).
33. Cornish, P.V., Ermolenko, D.N., Noller, H.F. & Ha, T. Spontaneous intersubunit rotation in single ribosomes. *Mol. Cell* **30**, 578–588 (2008).

ONLINE METHODS

Microarray analysis of *prp2-1* versus wild type. To find a yeast pre-mRNA that is active *in vitro* and that has a small intron, we performed the experiment described in detail in **Supplementary Methods**. We monitored the presence of spliced mRNA by hybridization of a fluorescent cDNA copy of the mRNA to an immobilized DNA fragment whose sequence spans the spliced junction. Characterization of this microarray assay is described in previous work[16]. The splicing of most yeast introns is inhibited in the mutant *prp2-1* at the nonpermissive temperature[16]. We selected *UBC4* from among the top candidates from this microarray (see **Supplementary Table 1**).

Synthesis and activity of Ubc4 pre-mRNA substrates. The two oligonucleotides that comprise the Ubc4 pre-mRNA substrate, the 5′ segment of 76 nt and the 3′ segment of 59 nt, each containing a single 5-aminoallyl uridine, were synthesized by Dharmacon. Mutant versions of these oligonucleotides were also synthesized (**Supplementary Table 2**). We deprotected half of each synthesis at a time and then purified each by electrophoresis on a denaturing, 7 M urea, 6% (w/v) polyacrylamide gel. We identified the bands by UV shadowing and eluted them by overnight (~16h) rotation in 0.3 M sodium acetate, pH 5.5, 1 mM EDTA, 0.1% (w/v) SDS. Following elution, we removed the gel fragments by centrifugation, extracted the supernatant with phenol-chloroform and precipitated the RNA ethanol. It is important to remove all Tris in this step because it can interfere with dye conjugation. For coupling, we resuspended 2–5 nmol of each fragment in 40 µl of 0.1 M sodium bicarbonate buffer, pH 9.0, and incubated them for 60 min at 60 °C with one dye pack of the *N*-hydroxysuccinimidyl ester dissolved in DMSO. We reacted the 5′ and 3′ fragments with Cy3 and Cy5 *N*-hydroxysuccinimidyl ester, respectively. After dye coupling, we ethanol-precipitated the conjugated fragments, washed them until ethanol-soluble dye was removed and then purified them on a denaturing, 7 M urea, 20% (w/v) polyacrylamide gel. We eluted the conjugated oligonucleotide from the gel by overnight (~16h) rotation and subsequently purified it as described above. The overall yield of coupled oligonucleotide was generally ~2–5 nmol. We ligated the purified and conjugated oligonucleotides as described[34] using T4 RNA ligase I and a DNA splint (dSplint) from Integrated DNA Technologies. We separated the ligated fragments by gel electrophoresis and eluted them as described above. The overall yield in this step is only 10–20%, but the resulting 200–500 pmol suffice for a large number of smFRET experiments.

The 135-nt version of the *Ubc4* pre-mRNA with a 95-nt intron and 20-nt 5′ and 3′ exons has the 5-aminoallyl uridine residues in the 5′ exon and in the 3′ exon (positions −7 and +4, depicted in bold font in **Supplementary Table 2**). In the 3′SS mutant, we replaced the bold underlined guanine with a cytosine. In the BP mutant, the italicized underlined adenosine is replaced by a cytosine. We determined the splicing activity of this fluorescently labeled Ubc4 pre-mRNA using standard *in vitro* assays, wherein we incubated 5–10 fmol of Ubc4 pre-mRNA at a final concentration of 0.2 nM in 40% (v/v) yeast whole-cell extract containing 8 mM HEPES-KOH, pH 7.0, 2 mM $MgCl_2$, 0.08 mM EDTA, 60 mM $K_i(PO_4)$, 20 mM KCl, 8% (v/v) glycerol, 3% (w/v) PEG and 0.5 mM DTT, supplemented with 2 mM ATP, and we resolved the products via denaturing PAGE and scanned them on a Typhoon variable mode imager. All sequences for substrates and oligonucleotides used in this study are available in **Supplementary Table 2**.

Preparation of yeast cell extract. We prepared splicing active whole-cell extract as described previously for BJ2168 yeast cells[35] with the following exceptions. We grew cells in 8–16 l yeast extract peptone dextrose medium to an OD_{600} of 2.5–3.0. We then harvested and washed the cells. We obtained pellets of a thick slurry of the extract by dripping the slurry into liquid nitrogen. These pellets can be frozen at −70 °C for further use. We disrupted the cell pellets by grinding them in a ball mill grinder (RMM301, Retsch) for five cycles of 3 min at 10 Hz. Between each cycle, we cooled the canisters in liquid nitrogen. We thawed the frozen powder in an ice bucket and centrifuged it at 34,950*g* in a Ja-25 Beckman rotor; we then centrifuged the supernatant at 100,000*g* in a Ti-60 rotor for 1 h. We removed the clear middle layer using a syringe and then dialyzed this extract for 4 h against 20 mM HEPES-KOH, pH 7.0, 0.2 mM EDTA, 0.5 mM DTT, 50 mM KCl, 20% (v/v) glycerol with one buffer exchange. We used 40% (v/v) cell extract in all assays and in all single-molecule studies. We achieved ATP depletion by adding 1 mM glucose to the cell extract and incubating it at room temperature (21–24 °C) before each experiment.

Single-molecule FRET. We prepared slides using a protocol modified from previous published methods[36,37]. We reacted quartz slides with aminopropyltriethoxysilane in acetone for 30 min to generate an amino-functionalized surface, we reacted which overnight (~12h) with a 10:1 mixture of succinimidyl ester–functionalized *O*-methyl-PEG and biotin-PEG to PEGylate the surface. We reacted sulfo-disuccinimidyl tartrate for 30 min with the remaining unreacted amines, thus ensuring the surface did not carry a positive charge. Slide coverslips underwent a similar procedure. We then rinsed and dried the slides and then assembled a single flow channel per slide. We added a solution of 0.2 mg ml^{-1} streptavidin in buffer (50 mM Tris-HCl, pH 7.5, 50 mM NaCl) to the channel and incubated it for 10 min at room temperature.

We heat-annealed the doubly labeled pre-mRNA to a 2′-*O*-methyl-RNA capture (tether) strand complementary to the 17 3′-terminal nucleotides of the 3′ exon by incubating it at 70 °C for 2 min and cooling it to room temperature for 10 min. The tether strand carries a 5′ biotin, which binds to the streptavidin on the surface of the slide to immobilize the pre-mRNA. After tether annealing, we diluted the hybrid to a concentration of ~50 pM in 100 µl splicing buffer, flowed it into the slide and incubated it for 10 min. Using a prism-based TIRF microscope as described[38], we collected data from single molecules in splicing buffer (8 mM HEPES-KOH, pH 7.0, 2 mM $MgCl_2$, 0.08 mM EDTA, 60 mM $K_i(PO_4)$, 20 mM KCl, 8% (v/v) glycerol, 3% (w/v) PEG, 0.5 mM DTT), 40% (v/v) cell extract depleted of ATP or 40% (v/v) cell extract supplemented with 2 mM ATP, both extracts in splicing buffer. We added an oxygen scavenger system composed of protocatechuate dioxygenase and protocatechuate to splicing buffer and cell extracts to limit photobleaching[26]; we also added Trolox to the solution to limit fluorophore blinking[39]. We excited the Cy3 donor using a 532-nm laser, and we recorded emission by the Cy3 and Cy5 fluorophores at 100-ms time resolution using an intensified CCD camera (Princeton Instruments, I–Pentamax). We then calculated a FRET value by dividing the intensity of acceptor emission by the total emission from both donor and acceptor. It should be noted that our ability to observe FRET transitions has a lower boundary imposed by our TIRFM time resolution of 100 ms and an upper boundary derived from the time window before either of the fluorophores photobleaches (~100 s). This dynamic range of ~4 orders of magnitude resolves many, but probably not all, kinetic differences among the pre-mRNAs, especially in light of the slow splicing kinetics *in vitro*. To further extend our observation time window, we therefore performed experiments involving extended pre-incubation with splicing active extract before commencing high-resolution (100 ms) smFRET detection.

We detected anticorrelation in two ways. First, we prefiltered trajectories to be studied by searching for the presence of any substantial anticorrelation by visual inspection. Second, we screened transition events found within the prefiltered FRET index trajectories for localized anticorrelation in the donor and acceptor traces. The postfiltering system required the use of the HMM tools in the QuB software suite (http://www.qub.buffalo.edu/soft.php) on the prefiltered data. We independently modeled the raw donor, acceptor and FRET indices to determine transition boundaries using a global fitting routine that simultaneously analyzes all data points in a given experimental condition (**Supplementary Fig. 2**). We coded and executed the postfilter algorithm in a MATLAB environment. Alternatively, we carried out a preliminary analysis of individual trajectories in which we explicitly optimized the rates of FRET transitions as in previous single-molecule FRET analysis[23,24]. Consistently, this analysis identified similar sequence and ATP-dependent changes. However, the large number of FRET states and trajectories in our datasets and the apparent kinetic heterogeneity ultimately resulted in a lower level of confidence in the resulting transition models. In-depth discussion of HMM analysis is in **Supplementary Methods**.

Verification of splicing *in situ* by RNase H probing. We immobilized each Ubc4 construct (WT, BP and 3′SS mRNA) on a quartz slide, incubated the slide with splicing buffer, ATP-depleted extract or ATP-supplemented extract, and monitored each by smFRET as described above. We washed out extract with 100 µl 1 M NaCl solution and incubation over 2 min, repeated three times. Following the final wash, we equilibrated the sample chamber with 100 µl RNase H buffer (20 mM HEPES-KOH, pH 7.8, at 25 °C, 1 mM DTT, 50 mM KCl, 50% (v/v) glycerol, 0.2 mg ml^{-1} BSA) for 5 min, followed by incubation for 20 min with 100 µl 250 µM deoxyoligonucleotide dRH, which is complementary to the Ubc4 intron in RNase H buffer. Next, a movie was taken for 50 frames with direct excitation of both Cy3 and Cy5 ('before RNase H'). We then washed the slide with 100 µl 250 µM dRH and 10 U RNase H (Promega) in RNase H buffer, incubated it for 30 min and washed it again with 100 µl 250 µM

dRH in RNase H buffer. A second movie was taken as above ('after RNase H'). We quantified movies collected before and after RNase H treatment using an in-house spot-finder algorithm, which uses a second-order nonlinear polynomial equation to correctly align the Cy3 and Cy5 channels, and determined the number of diffraction-limited points in each channel using a reference bead slide for calibration[39].

34. Stark, M.R., Pleiss, J.A., Deras, M., Scaringe, S.A. & Rader, S.D. An RNA ligase–mediated method for the efficient creation of large, synthetic RNAs. *RNA* **12**, 2014–2019 (2006).
35. Stevens, S.W. & Abelson, J. Yeast pre-mRNA splicing: methods, mechanisms, and machinery. *Methods Enzymol.* **351**, 200–220 (2002).
36. Ha, T. *et al.* Initiation and re-initiation of DNA unwinding by the *Escherichia coli* Rep helicase. *Nature* **419**, 638–641 (2002).
37. van Oijen, A.M. *et al.* Single-molecule kinetics of lambda exonuclease reveal base dependence and dynamic disorder. *Science* **301**, 1235–1238 (2003).
38. Zhuang, X. *et al.* Correlating structural dynamics and function in single ribozyme molecules. *Science* **296**, 1473–1476 (2002).
39. Rasnik, I., McKinney, S.A. & Ha, T. Nonblinking and long-lasting single-molecule fluorescence imaging. *Nat. Methods* **3**, 891–893 (2006).

doi:10.1038/nsmb.1767